Improved sensitivity gas detection by spontaneous Raman scattering

Michael P. Buric,[1,2] Kevin P. Chen,[1,2] Joel Falk,[1,2,*] and Steven D. Woodruff[1]

[1]National Energy Technology Laboratory, 3610 Collins Ferry Road, Morgantown, West Virginia 26507, USA

[2]Department of Electrical and Computer Engineering, University of Pittsburgh, 348 Benedum Hall, Pittsburgh, Pennsylvania 15261, USA

*Corresponding author: falk@engr.pitt.edu

Received 30 April 2009; revised 1 July 2009; accepted 6 July 2009; posted 14 July 2009 (Doc. ID 110699); published 24 July 2009

Accurate, real-time measurement of the dilute constituents of a gaseous mixture poses a significant challenge usually relegated to mass spectrometry. Here, spontaneous Raman backscattering is used to detect low pressure molecular gases. Rapid detection of gases in the ~100 parts in 10^6 (ppm) range is described. Improved sensitivity is brought about by use of a hollow-core, photonic bandgap fiber gas cell in the backscattering configuration to increase collection efficiency and an image-plane aperture to greatly reduce silica-Raman background noise. Spatial and spectral properties of the silica noise were examined with a two-dimensional CCD detector array. © 2009 Optical Society of America

OCIS codes: 300.6450, 060.5295.

1. Introduction

Hollow-core photonic bandgap fibers (HCPBFs) offer a number of exciting opportunities for optical gas sensing. Single-mode, low-loss optical guiding in the hollow core allows a long interaction length between an optical pump beam and the gas species to be analyzed. Gas sensing based on absorption or on spontaneous forward-scattering Raman spectroscopy in such fibers has been demonstrated [1,2]. The intrinsic advantages of HCPBFs for sensing, together with their robust structure, make these fibers natural candidates for high-temperature (400 °C) chemical sensing applications. These applications include real-time natural gas and syngas composition analysis in reactors and combustors [3–5]. Although experimental Raman-based results are promising, gas sensing in HCPBF is limited by a background silica-Raman signal. The Raman cross section of solid silica glass is many times larger than that of any gas species, and amorphous silica exhibits a wide continuous Raman spectrum [2,6]. The presence of silica Raman drastically reduces the detection sensitivity and usefulness of HCPBF-based sensing.

We demonstrate that the silica Raman is generated in the fiber cladding and report a method of minimizing this noise. The Raman output generated in the silica cladding is guided by surface modes [7], and these modes can be spatially separated from the Raman signal generated by gas constituents in the hollow core. An aperture at an image plane of the fiber's output can be used to block the silica Raman. In a visible wavelength-pumped system, we report a reduction of the detected silica-Raman output by nearly 2 orders of magnitude when a properly sized image-plane aperture is introduced. This reduction was observed without a significant change in the gas-Raman signal. In a similar infrared experiment, we examined the spatial and spectral profile of the silica Raman to further demonstrate the separability of silica-Raman noise from gas-Raman signals using a two-dimensional CCD array instead of a pinhole spatial filter.

2. Experiments

The two Raman HCPBF-based gas-sensing systems investigated, shown schematically in Fig. 1, use

0003-6935/09/224424-06$15.00/0

backward-wave Raman scattering arrangements for gas detection. Both laser input and Stokes output (backward wave) occur at the same end of the fiber. This configuration leaves the other end of the fiber free for gas input with no optical coupling requirements at that end of the fiber. In contrast with a previously reported forward-wave Raman gas-sensing experiment [2], the backscattering arrangement uses the same optic to couple the pump light into the fiber as is used to collect the Raman output. This means that, in the absence of significant chromatic aberration in the coupling lens, alignment at the pump wavelength leads to alignment at the Stokes wavelength. Additionally, in the case of a HCPBF with significant loss, the backward wave configuration also produces a larger Raman signal [8]. All the fibers exhibit some transmission loss, and the least attenuated portion of the pump beam generates the strongest Raman signal. In the backward configuration, the strongest portion of the generated Raman signal also emerges with the least attenuation. In contrast, in forward Raman scattering, the strongest generated signal experiences the most loss. For example, if a fiber of length L has a (power) loss coefficient at both Stokes and pump wavelengths of α, then the backward-wave configuration produces a signal that is

$$\frac{\sinh(\alpha L)}{\alpha L} \tag{1}$$

times stronger than that obtained from the forward-wave configuration [8].

The sensitivity of the gas detection system is critically dependent on minimization of system noise. Earlier work in a forward Raman scattering HCPBF system showed that the most significant source of noise was a strong band of amorphous silica-Raman scattering. This scattering starts near the pump frequency and has an amplitude that generally decreases with spectral shift from the pump. Silica Raman is observed as far away as 2500 cm^{-1} from the pump frequency. The (spectrally) integrated silica-Raman scattering cross section is many times larger than that of a typical molecular gas [2].

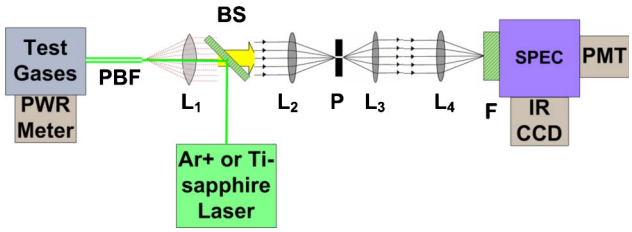

Fig. 1. (Color online) Experimental setup: L_1, 11 mm aspheric singlet; L_2, 14 mm aspheric singlet; L_3, 25 mm spherical singlet, P, pinhole; L_4, 6 cm EFL spherical singlet; BS, dichroic long-pass beam splitter; SPEC, 0.55 m grating spectrometer; PMT, EMI 9789A photomultiplier with photon counting; IR CCD, EG&G 1421 IR 1024 element CCD array or Princeton Instruments SpectruMM 250B with Hamamatsu MPP backilluminated 1024 × 252 element sensor array.

The silica-Raman signal is produced by the small amount of pump light that propagates in the silica cladding. Approximately 5% of the transmitted optical power propagates in the cladding glass honeycomb [9,10]. Although a Gaussian-like mode dominates propagation in the fiber core, additional higher-order surface or interface modes exist [7]. These modes propagate in the cladding structure and are the sources of the silica-Raman signal that obscure the weak gas-Raman signal. Fortunately, these surface modes have a spatial profile amenable to reduction by careful aperturing. Because their mode profiles do not strongly overlap the core, the Raman signal that they produce can be minimized with little effect on the gas-Raman signatures.

To investigate Raman-based gas detection, two HCPBF Raman gas cells were assembled as shown in Fig. 1. One system used a visible gas argon-ion laser pump, the other a near-IR, Ti:sapphire laser pump.

A. Visible Laser-Pumped System

In the visible laser-pumped system, ~100 mW of 514.5 nm TEM_{00} argon-ion laser light was reflected into an 11 mm effective focal length (EFL) aspheric singlet (L_1) with a dichroic beam splitter [11]. The focused beam was coupled into a 1 m length of HC-580 HCPBF [9] using a three-axis nanopositioning stage. More than 60% power throughput was obtained. Pump propagation loss was approximately 20% and the remaining loss was coupling loss that is due to mode mismatch and imperfections in the cleaved fiber facet. Pump light reflected from the fiber is rejected by our detection system and does not affect gas detection sensitivity. Decreasing coupling efficiency, however, often leads to increasing the power in higher-order surface modes, thus resulting in increased silica-Raman noise. This indicates the importance of maximizing coupling efficiency to achieve the lowest possible noise floor. The backscattered spontaneous Raman that emerged at the same end of the fiber as the input pump beam was recollimated by the coupling lens and passed with slight attenuation through the dichroic beam splitter. In contrast with a previously reported PBF forward Raman-scattering system, this configuration provided a simple means to introduce test gases or to evacuate the fiber at the other (nonoptical) end [2]. That end of the fiber was terminated in a 1/16 in. (0.159 cm) Swagelok fitting using a graphite ferrule with a 300 μm bore.

The collimated Raman beam that emerged from the coupling lens was initially focused into a 0.55 m focal length grating spectrometer with a 6 cm EFL lens. Stokes signals in the visible range were measured with either a photomultiplier tube (PMT) (EMI 9789A) or a multialkali photocathode, proximity-focused multichannel plate intensifier whose phosphor plate was fiber coupled to a silicon reticon (EG&G 1421 IR). Both detectors operated in a photon counting mode. The PMT output was connected to a

discriminator that provided a voltage output for data recording at $1\,V/10^5$ counts. During initial experiments, the fiber gas cells contained only ambient air. A large amorphous silica-Raman band (Fig. 2) was noted to exhibit a distribution nearly identical to that previously noted in solid-core PBF [12] along with the characteristic peaks from nitrogen ($2331\,cm^{-1}$) and oxygen ($1556\,cm^{-1}$). The silica-Raman-related peaks visible in Fig. 2(b) are similar to those shown in [12]. The peak at ~537 nm, $802\,cm^{-1}$ away from the pump wavelength, is identified as a Si–O–Si bending Raman mode and the peak at ~544 nm, $1048\,cm^{-1}$ from the pump wavelength, is a Si–O stretch Raman mode.

A spatial filtering apparatus (shown in Fig. 1) was inserted between the beam splitter and the input lens of the spectrometer. The filter consisted of an $L_2 = 14$ mm EFL aspheric singlet and a pinhole. The combination of the 11 mm focal length lens (Fig. 1, L_1) and L_2 formed a magnified image (magnification of $M = 14/11 = 1.27$) of the fiber's output face located at an image plane approximately 14 mm from L_2. The position of the pinhole was optimized to maximize gas-Raman throughput, which corresponds to formation of an image of the fiber end facet at the pinhole. The pinhole allowed transmission of the near-Gaussian profile gas-Raman mode propagating in the fiber's core; eliminating modal content from the silica Raman propagating outside the hollow core, the diameters of pinholes investigated experimentally ranged from 5 to 20 μm.

Figure 2 shows spectra measured in the visible Raman system with and without a 10 μm diameter pinhole. The spectrometer slits were 0.2 mm wide, yielding approximately 0.27 nm resolution. The nitrogen gas-Raman signal was reduced by approximately only 6% with the addition of the 10 μm pinhole [13]. The silica-Raman output, however, was reduced by at least 2 orders of magnitude over the entire band. It was also observed that pinholes smaller than 10 μm reduced both the silica- and the gas-Raman signals. Pinholes larger than 10 μm diameter resulted in a lesser reduction of silica Raman, with no effects on gas-Raman signals. These results are sensible given the imaging properties of the system. The mode field diameter ($1/e$) that emerged from the fiber is 4.9 μm. This mode is magnified 1.27 times by the combination of L_1 and L_2 (and becomes ~6.2 μm wide). This indicates that a 5 μm pinhole would remove a significant portion of the gas-Raman mode, whereas a 10 μm pinhole would pass most of the gas Raman. If the system were to be perfectly optimized to maximize gas Raman and to minimize silica-Raman noise, a magnification and pinhole would be chosen to exactly match the core-mode size with no underfilling or overfilling. Despite the exponentially radially decaying nature of these modes and the complexity of their distributions, near-optimized filtering can be accomplished aperturing just outside the 99% power point of the gas-Raman core mode.

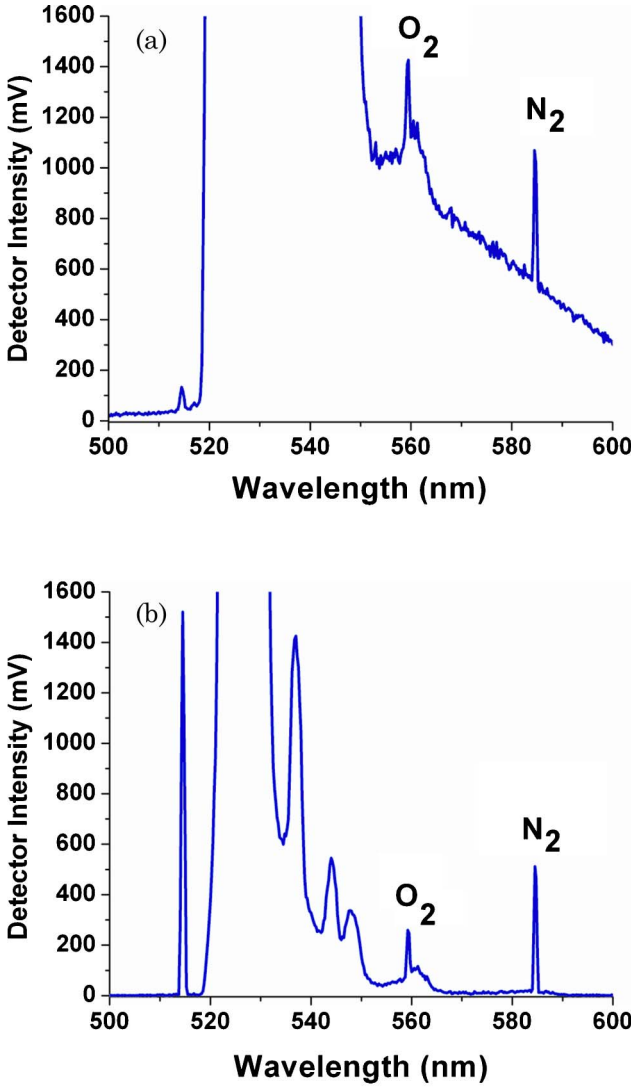

Fig. 2. (Color online) (a) HCPBF spectrum from ambient air. No image plane aperture. (b) 10 μm diameter image plane aperture added (bottom). Signals were recorded with PMT photon counting at $1\,V/10^5$ counts.

After determining the optimal size of the filtering pinhole, the Raman signal was measured with and without the spatial filter. The prominent Stokes nitrogen signal at $2331\,cm^{-1}$ was used to establish detection limits. If C_{gas} represents the number of detected photoelectron counts/second above the background at the 584.5 nm nitrogen Raman wavelength, the number of signal photoelectrons produced in a detector integration time τ is $C_{gas}\tau$. The limiting system noise is quantum noise caused by the discrete emission times of signal (gas-Raman) photoelectrons, those produced by silica Raman and detector dark current. If C_{Si} represents the number of detected background (silica-Raman plus dark current) photoelectron counts/second and if $C_{Si} \gg C_{gas}$, then the signal-to-noise ratio (SNR) is determined by [14]

$$\mathrm{SNR} = \frac{C_{gas}\tau}{\sqrt{C_{Si}\tau}}. \quad (2)$$

Equation (2) assumes that the background is Poisson distributed and can be subtracted out, but the fluctuation of the background signal remains as noise. The minimum detectable C_{gas} is estimated from a SNR of 1 or for the 1 s integration time employed in our experiments $C_{gas_{\min}} = \sqrt{C_{\mathrm{Si}}}$. The value $R = C_{gas}/C_{gas_{\min}}$ indicates by what factor the gas pressure could be reduced before achieving a SNR of 1. The value of R without the spatial filter is approximately $230(1 \pm 0.1)$. The use of a 10 μm diameter pinhole increased R to $1380(1 \pm 0.1)$. (Error estimates are based on laser power fluctuations and the observed variations in laser coupling efficiencies over a multiminute time frame.) Based on the known concentration of nitrogen in the atmosphere, we calculate that this improvement should permit N_2 detection (a SNR of 1) in a gas mixture at less than 565 parts in 10^6 (ppm). Because detector noise is approximately 2 orders of magnitude lower than the silica-Raman signal, we estimate that less than 0.1 s sampling time can be used without a large reduction in R. Furthermore, we can also show that the time taken to introduce gases into the fiber core is at least several times the sampling period at reasonable (<7 MPa) input gas pressures [15].

A goal of the research reported here was to use this gas-Raman system for measurement of the constituent components of natural gas or syngas (synthetic fuel gases made from coal). Figure 3 shows the Raman signal concentration dependence from one hydrocarbon (methane) and from a major component of syngas (carbon dioxide). Figure 3 shows the variation of the methane Raman signal magnitude at 2917 cm^{-1} and the syngas CO_2 Raman signal magnitude at 1388 cm^{-1} with gas pressure. Integration time was 1 s for each measurement. To explore the sensitivity of the current Raman detection configuration, the pump-light input end of the fiber was fitted with a sealed flange and fused silica window. A vacuum was applied to the flange; dropping the gas pressure at this end of the fiber to less than ~130 mPa. This technique did not significantly reduce optical coupling efficiency but provided constant gas flow through the fiber. Test gases were then introduced at the opposite fiber end at pressures from a few pascals to greater than 700 kPa (~100 psig). The Fig. 3 inset is a record of the detection of methane at an input pressure of 33 Pa. Integration time was increased to 20 s to increase the visual clarity of the inset, although electronic detection in 1 s is possible at this pressure. The value of R in the inset is approximately 4.5 or $\sqrt{20}$, which indicates a value of $R = 1.0$ for a 1 s integration time. The noise in the inset is due to silica Raman, which exhibits a small local minimum at the left-hand side of Fig. 3, unrelated to the overall trend of silica Raman decreasing toward longer wavelengths. The average methane density in the fiber was equal to that which would occur with a methane concentration of 164 ppm in atmospheric pressure. It should be noted that before each measurement, the gas input end of the PBF was also evacuated to ~130 mPa. This was necessary to remove any residual gas trapped in the HCPBF and gas manifold to produce an accurate concentration measurement.

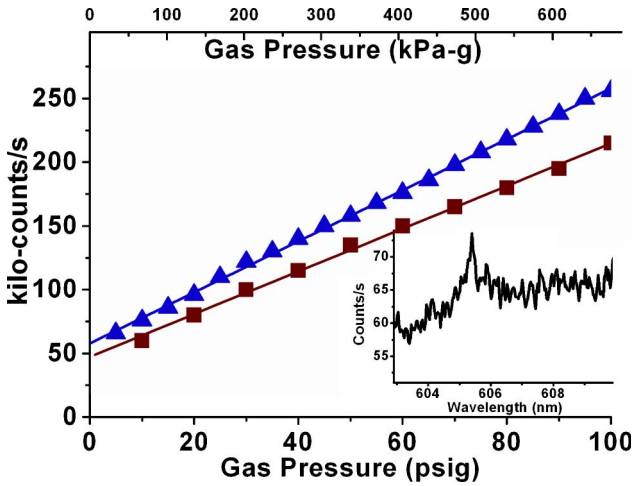

Fig. 3. (Color online) Raman signal strengths, methane (■) at 2917 cm^{-1} (85 mW pump power) and CO_2 (◀) at 1388 cm^{-1} (65 mW pump power) versus fiber input gas pressure. The EG&G CCD array detector was used for this measurement. The inset shows detection of 33 Pa (equivalent to 164 ppm in air) of methane as described in the text. For the data shown in the inset, the detection integration time was increased to 20 s for clarity.

We note that the ratio of methane to carbon dioxide signal magnitudes or line slopes shown in Fig. 3 is not equal to the ratio of Raman cross sections of these gases, which predicts a methane signal approximately four times that of carbon dioxide for equal pump powers and pressures [16]. The data shown in Fig. 3 were taken in a way that makes direct comparison of the two gas signals or line slopes impossible. Spectrometer slit widths were reduced to minimize system noise that is due to light scattered inside the spectrometer and other noise observed at low gas pressures. This resulted in a loss of collected Raman signal due to imperfect alignment and/or optical aberrations in the collection optics train (Fig. 1, L_1–L_4). These losses were not the same in the methane and carbon dioxide measurements. We also note that our detector is approximately 25% more sensitive at the CO_2 Stokes wavelength than at the methane Raman wavelength. Figure 3 is only intended to demonstrate the linear variation of Raman signal with gas pressure and not to measure relative cross sections. Furthermore, it should be noted that both lines cross the x axis at the point at which the average internal fiber pressure is zero or at approximately −30 psig applied pressure in Fig. 3.

Limits to gas detection sensitivity are based on the level of silica-Raman noise at the Stokes wavelength of interest. Silica-Raman noise, in general, decreases with increasing spectral separation from the pump wavelength. This means that gases with large Stokes shifts inside the fiber's transmission band should have higher detection sensitivity. Based on the observed silica-Raman noise near a Stokes line and the

Raman cross section of the corresponding analyte gas, the detection limits of various species can be easily calculated [5,16]. Using the silica-Raman background signal recorded in our optimized system along with recorded atmospheric gas-Raman magnitudes [Figs. 1 and 2(b)], we calculate a minimum detectable concentration of less than 20 ppm for both ethane (2914 cm^{-1}) and propane (2906 cm^{-1}). These calculations assume 1 s integration times. Some improvement beyond these limits is possible by carefully reducing the amount of collected silica Raman by further reducing the spectrometer input slit so that a minimum of spectrally broad silica noise is collected. For example, a reduction in silica-Raman noise by $\sqrt{10}$ should be achievable by reducing the spectrometer slit used to record the data in Fig. 2 from 200 to 20 μm. A reduction of slit width comes at the expense of increased difficulty in system alignment.

B. Infrared Laser-Pumped System

To further characterize the noise in the HCPBF Raman system, we used a two- dimensional silicon detector array (Princeton Instruments SpectruMM 250B with a Hamamatsu multipinned phase backilluminated 1024×252 element sensor array with $24\,\mu m \times 24\,\mu m$ pixels) to examine the spatial and spectral content of the light exiting from a 5 m length of HC-800-01 PBF pumped with an ~780 nm Ti:sapphire laser; itself pumped by an argon laser. The fiber has a core diameter of approximately 9.3 μm [10] and a full photonic bandgap (high transmission range) extending from approximately 770 to 890 nm. The fiber loss over this range is less than 0.5 dB/m. The optical components employed are similar to those shown in Fig. 1, although the L_2, L_3, and P were removed, and the PMT used in the visible experiments was replaced by the two-dimensional silicon array. Raman scattering measurements were first made with the fiber filled with ambient air. The (1556 cm^{-1}) oxygen Raman line lies well within the fiber passband, so it was used to make detailed comparisons between spatial and spectral components in gas and silica Raman. Focusing lens L_4 shown in Fig. 1 ($f = 6$ cm) produces a magnified image of the fiber output on the spectrometer input slit. Magnification M is the ratio of the focal lengths of L_4/L_1 or $60/11 = 5.5$. Transmission through the 0.55 m focal length spectrometer maintains this magnification in the vertical direction but spectrally disperses the fiber output in the horizontal dimension. The output image is recorded by the silicon array. The magnified images of the fiber core, cladding, and solid silica regions have diameters of approximately 51, 220, and 743 μm; i.e., they extend over 3, 10, and 31 vertical array elements, respectively. The dispersion of the spectrometer is 1.37 nm/mm or 0.034 nm/array element. The input slit was set at 200 μm width and 1 mm height. The image in Fig. 4 shows a contrast-enhanced output from the two-dimensional array. The center bright spot is due to

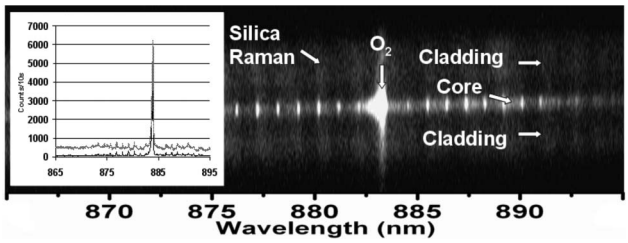

Fig. 4. Raman signal strengths with 780 nm pumping. The photograph is an image of the spectral and spatial extent of the light scattering observed in the core, holey cladding, and a small portion of the surrounding solid silica. For figure clarity, a double thresholding algorithm was applied in which pixels with values less than 5 counts were eliminated and pixels with values greater than 50 counts were displayed as maximum intensity. The inset shows spectra of the scattered light emerging from the core and the core plus cladding (see text).

Raman scattering from oxygen. The nearly evenly spaced vertical spectral lines (spacing of ~1.0 nm) are the rotational substructure of the Stokes scattering [17]. The locations of the fiber core and cladding images are indicated. The broad spectral scattering observed in the photo is caused by Raman scattering in the silica located outside the core. The inset shows two spectral displays of the scattered light (10 s integration times) as functions of wavelength. The lower trace is a sum of the counts in the three central rows of pixels; i.e., the lower trace represents the total signal propagating in the fiber core. The upper trace is a sum of the counts in the center 31 rows of pixels (the figure displays approximately 50 rows of pixels in the vertical direction); i.e., the total signal transmitted in the PBF core and cladding. For both displays, dark current was subtracted. The ratio $R = C_{gas}/C_{gas_{min}}$ indicated by the core signal is approximately 500. The ratio (R) for the entire PBF signal (top trace in the inset) is significantly worse (≈275) due to the summing of silica noise, as would occur in a single element detector system with no spatial filtering. In effect, the two-dimensional array serves as a kind of digital spatial filter by selectively utilizing the desired portion of the array image. The spectral resolution in Fig. 4 is limited by the 200 μm wide input slit width. The wide slit width was used for ease of alignment and to ensure imaging of both the fiber core and the cladding.

3. Conclusions

We have reported the observation of gas-phase spontaneous Raman backscattering with enhanced signals, reduced noise, and improved gas detection limits using a photonic bandgap fiber as a gas cell and collection optic. Larger gas-Raman signals were recorded using this backscattering system than in previously reported forward-scattering experiments [2]. Noise in this system was shown to be largely due to silica-Raman scattering outside the fiber core. The photonic bandgap fiber gas cell provided a large interaction length for Raman backscatter, which was exploited usefully as a gas sensor by reducing silica-Raman noise with an image-plane aperture. In

general, this system can be used for the detection of any gas that has a Stokes wavelength within the $\sim 2500\,\mathrm{cm}^{-1}$ transmission band of the HCPBF.

This technical effort was performed by support of the Department of Energy, National Energy Technology Laboratory research in Energy Systems and Dynamics under Research and Development Support (RDS) contract DE-AC26-04NT41817 and from a National Science Foundation (NSF) grant 0639234. The authors thank Bruce Kang of West Virginia University for the loan of the two-dimensional detector array.

References and Notes

1. T. Ritari, J. Tuominen, H. Ludvigsen, J. C. Petersen, T. Sørensen, T. P. Hansen, and H. R. Simonsen, "Gas sensing using air-guiding photonic bandgap fibers," Opt. Express **12**, 4080–4087 (2004).
2. M. P. Buric, K. P. Chen, J. Falk, and S. D. Woodruff, "Enhanced spontaneous Raman scattering and gas composition analysis using a photonic bandgap fiber," Appl. Opt. **47**, 4255–4261 (2008).
3. X. Cao and C. N. Hefwitt, "Detection methods for the analysis of biogenic non-methane hydrocarbons in air," J. Chromatogr. A **710**, 39–50 (1995).
4. M. R. Beychok, "Coal gasification and the Phenosolvan process," presented at the 168th National Meeting of the American Chemical Society, Atlantic City, 8–13 September 1974 (American Chemical Society, 1974); FUEL 33.
5. J. Kiefer, T. Seeger, S. Steuer, S. Schorsch, M. C. Weikl, and A. Leipertz, "Design and characterization of a Raman scattering—based sensor system for temporally resolved gas analysis and its application in a gas turbine power plant," Meas. Sci. Technol. **19**, 085408 (2008),
6. B. E. A. Saleh and M. C. Teich, *Fundamentals of Photonics*, 2nd ed. (Wiley-Interscience, 2007). p. 554.
7. N. V. Wilding, P. S. Light, F. Couny, and F. Benabid, "Experimental comparison of electromagnetic induced transparency in acetylene-filled kagomé and triangular lattice hollow core photonic crystal fiber," in *Conference on Lasers and Electro-Optics* (Optical Society of America, 2008), paper JFA3.
8. S. Afshar V., Y. Ruan, S. C. Warren-Smith, and T. M. Monro, "Enhanced fluorescence sensing using microstructured optical fibers: a comparison of forward and backward collection modes," Opt. Lett. **33**, 1473–1475 (2008).
9. HC-580 HC-PBF data sheet retrieved 3 September 2008 from http://www.i-waveco.com/category/pdf/5131-HC58001.pdf.
10. HC-800-01 HC-PBF data sheet retrieved 3 November 2008 from http://www.crystal-fibre.com/datasheets/HC-800-01.pdf,
11. Semrock beam splitter data sheet. Downloaded 23 July 2008 from http://www.semrock.com/Catalog/RamanEdgeDichroic.htm.
12. D. Pristinski and H. Du, "Solid-core photonic crystal fiber as a Raman spectroscopy platform with a silica core as an internal reference," Opt. Lett. **31**, 3246–3248 (2006).
13. The 14 mm lens focusing into the pinhole plane exhibited significant chromatic aberration so that the oxygen Raman signal shown in Fig. 2 was reduced by approximately 43% with the addition of the pinhole. Later experiments utilizing an achromatic-doublet lens resulted in little attenuation at both wavelengths with the addition of the aperture.
14. R. W. Boyd, *Radiometry and the Detection of Optical Radiation* (Wiley, 1983), pp. 132–136.
15. J. Henningsen and J. Hald, "Dynamics of gas flow in hollow core photonic bandgap fibers," Appl. Opt. **47**, 2790–2797 (2008).
16. W. Fenner, H. A. Hyatt, J. M. Kellam, and S. P. S. Porto, "Raman cross section of some simple gases," J. Opt. Soc. Am. **63**, 73–77 (1973).
17. J. J. Barrett and N. I. Adams III, "Laser-excited rotation–vibration Raman scattering in ultra-small gas samples," J. Opt. Soc. Am. **58**, 311–318 (1968).